Journal of Materials Chemistry A

Accepted Manuscript

ROYAL SOCIETY OF CHEMISTRY

www.rsc.org/materialsA

Journal Name

ARTICLE

Brookite TiO_2 as low-temperature solution-processed mesoporous layer for hybrid perovskite solar cell

Received 00th January 20xx,
Accepted 00th January 20xx

DOI: 10.1039/x0xx00000x

www.rsc.org/

Atsushi Kogo*, Yoshitaka Sanehira, Masashi Ikegami and Tsutomu Miyasaka*

As solution-processable and low cost semiconductors, organolead halide perovskites are attracting enormous attention for promising photovoltaic absorbers, which is capable of high power conversion efficiency over 20%. Mesoporous layer of titanium oxide, which requires sintering process at high temperature (400–500 °C), serves as an efficient electron collector as well as scaffold of crystal nucleation. To enable rapid low cost manufacture and construction of lightweight flexible solar cells built on plastic film, sinter-free electron collection layer (mesoporous and compact layer) is required. In this study, highly crystalline layer of brookite (orthorhombic TiO_2) is prepared by sinter-free solution process as efficient mesoporous electron collector. Strong inter-particle necking of brookite nanoparticles by dehydration-condensation reaction enables formation of highly uniform mesoporous layer at low temperature (130–150 °C). In comparison with anatase TiO_2 meso-structure prepared by high temperature (500 °C) sintering, the brookite electron collector exhibits photovoltaic performance with greater fill factor and 100 mV-higher open-circuit voltage.

Introduction

Organic-inorganic hybrid perovskite materials represented by $CH_3NH_3PbI_3$ ($MAPbI_3$) have been intensively studied for high efficiency hybrid solar cells.[1-6] As solution-processable (printable) and low cost semiconductors, the hybrid perovskites are promising photovoltaic absorbers, which is capable of high power conversion efficiency (PCE) over 20%.[2] High efficiency is generally enabled by preparation of high quality void-less perovskite layer of uniform thickness and quality of underlying scaffold and charge transport layers that can hold perovskite with continuous junction. Here, mesoporous (mp) layer of metal oxide semiconductors serves as an efficient electron collector as well as scaffold of crystal nucleation.[6] Among metal oxides, TiO_2 have been the most extensively employed mp collector in junction with perovskite. Here, the crystalline form of TiO_2 ever studied was anatase or anatase-rich type (e.g., Degussa P-25), which is also the common TiO_2 semiconductor employed in dye-sensitized solar cells (DSSC). Unlike DSSC, however, morphology and surface property of mp TiO_2 layer as the scaffold have significant influence on the quality of the perovskite layer (e.g. crystal size, uniformity, surface coverage on the mp layer) that determine the photovoltaic performance. To date, anatase TiO_2,[3-5] rutile TiO_2,[7] ZnO,[8] SnO_2,[9] WO_3,[10] and $SrTiO_3$[11] have been examined for metal oxide electron collectors and scaffolds in perovskite solar cells. Anatase TiO_2 has been further studied for surface modification to improve contact between mp TiO_2 layer and perovskite layer.[12-14]

Formation of mp metal oxide films usually requires sintering process at high temperature (400–500 °C) by using a mesoscopic coating paste. To ensure inter-particle necking and adhesiveness of TiO_2 nanoparticles on a conductive glass, polymer binder is used as an additive in the precursor paste, which is to be removed after sintering to ensure high conductivity. In contrast, binder-free mesoscopic paste or slurry is required to develop sinter-free low temperature process for fabrication of solar cells. Such processes enable rapid low cost manufacture and construction of lightweight flexible solar cells built on plastic film.[8,15] However, low temperature process tends to limit the cell performance in terms of voltage and efficiency due to low carrier collection ability of TiO_2 in comparison with the high performance of sintered TiO_2 layers.

In this study, we employed brookite nano-TiO_2 crystal for mp scaffold and electron collector of perovskite solar cells for the first time. A significant merit of brookite TiO_2 is that high quality uniform mp-TiO_2 layer can be prepared by sinter-free solution process (<150 °C) from a binder-free precursor paste. The surface of highly crystalline brookite TiO_2 exhibits high affinity for inter-particle necking and enables formation of mp structure, through dehydration condensation reaction of surface hydroxyl groups, at temperature below 150 °C.[16] Further, brookite TiO_2 has conduction band (CB) edge potential slightly (0.01–0.19 eV) more negative than that of anatase TiO_2.[17] This property of brookite has achieved a higher open-circuit voltage (V_{OC}) in the liquid junction structure of DSSC.[18-20] In this report, we demonstrate that brookite TiO_2-based meso-

Graduate School of Engineering, Toin University of Yokohama, 1614 Kurogane-cho, Aoba, Yokohama, Kanagawa, 225-8503, Japan. E-mail: miyasaka@toin.ac.jp; kogo@toin.ac.jp; Tel: +81-45-974-5055

Electronic Supplementary Information (ESI) available: SEM images of brookite TiO_2, anatase TiO_2, and Al_2O_3 layers are provided. See DOI: 10.1039/x0xx00000x

structure functions as an excellent scaffold and electron collector for the hybrid perovskite, $MAPbI_{3-x}Cl_x$, prepared by one-step solution process and achieves photovoltaic performance in terms of high voltage and efficiency with hysteresis-less characteristics.

Experimental

A TiO_2 hole-blocking layer (anatase, thickness ~50 nm) as a common structure was formed on the surface of a FTO glass substrate (10 Ω sq^{-1}, Nihon Sheet Glass, 1.1 mm in thickness) by spray pyrolysis technique using a $Ti(acac)_2(OC_5H_7)_2$-containing ethanol solution at 500 °C. For complete low-temperature fabrication of perovskite solar cells, low-temperature processing of hole-blocking layer such as chemical vapour deposition[21,22] can be employed. However, in this study, the layer was prepared at high temperature for the purpose to compare conventional anatase TiO_2 mp layer, sintered at 500 °C on the blocking layer, with the brookite mp layer. An aqueous brookite TiO_2 slurry (PECC-B01, Peccell Technologies, Inc., particle size 10–20 nm) was diluted to 33 vol% with ethanol by addition of a small amount of ethylene glycol and spin-coated on the above blocking layer at 3000 rpm for 30 s. The substrate was dried at 130–150 °C for 1 h. To form anatase TiO_2 mp layer, a TiO_2 paste (18NR-T, Dyesol, particle size ~20 nm) was diluted to 25 wt% with ethanol and spin-coated on the compact layer at 4000 rpm for 30 s and the dried substrate was sintered at 500 °C for 1 h. For Al_2O_3 mp layer, an Al_2O_3 slurry (Aldrich, <50 nm in isopropanol) was diluted to 5 wt% with 2-propanol and spin-coated at 4000 rpm for 30 s and sintered at 500 °C.

A mixed solution of CH_3NH_3I (2.7 M) and $PbCl_2$ (0.9 M) in *N*,*N*-dimethylformamide were spin-coated on the above mp layer at 2000 rpm for 30 s and annealed at 100 °C for 90 min in dry air to form perovskite $MAPbI_{3-x}Cl_x$ layer. A 2,2',7,7'-tetrakis-(N,N-di-4-methoxyphenylamino)-9,9'-spirobifluorene (spiro-OMeTAD) solution in cholorobenzene (0.12 M) containing 0.034 M bis(trifluoromethane) sulfonamide lithium salt and 0.098 M 4-*tert*-butylpyridine was spin-coated at 4000 rpm for 30 s and aged overnight in dry air. Finally, Au was vapor-deposited on the top of spiro-OMeTAD as a counter electrode. Photovoltaic characteristics of all the devices with an active area of 0.09 cm^2 were measured with a Keithley 2400 source meter under 1 sun illumination by using a Peccell Technologies PEC-L01 solar simulator (AM 1.5 G, 100 mW cm^{-2}). The IPCE action spectra of device were measured in ambient air at room temperature on Peccell Technologies, PEC-S20 action spectrum measurement setup. For characterization of mp layer and perovskite layer, an X-ray diffractometer (D8 Discover, Brucker) with CuKα radiation source, a scanning electron microscope (SU8000, HITACHI) and an atomic force microscope (SPM-9500J3, SHIMADZU) were employed. Water contact angle was measured with a contact angle meter (CA-X, KYOWA).

Results and discussion

Aqueous mesoscopic precursor solution of brookite was prepared from a slurry of nano-crystalline brookite TiO_2 (supplied from Peccell Technologies, Inc., particle size, 10–20 nm) by homogeneous dispersion of brookite nanoparticles with a water/ethanol mixture by means of a rotation revolution mixer at temperatures of 20–35 °C. To avoid spontaneous aggregation of brookite nanoparticles, ethylene glycol was added to the mixture. The resultant precursor contained brookite TiO_2 at concentration of 5–8 wt %. For electrode fabrication, mesoporous brookite layer was built on a thin compact anatase TiO_2 layer. The brookite precursor solution was spin-coated on a thin anatase TiO_2 compact layer (~50 nm) that covers the surface of an F-doped SnO_2 (FTO) transparent conductive layer on glass substrate. The thickness of brookite meso-structure was ~250 nm. The substrate was subjected to drying under ambient air at 130–150 °C to cause dehydration condensation reaction at the surface of brookite nanoparticles leading to inter-particle bonding (-Ti-OH + HO-Ti- → -Ti-O-Ti + H_2O).[16] This simple drying treatment converted the brookite precursor to a mp brookite layer. Fig. 1a shows a scanning electron microscopy (SEM) image of mp brookite layer thus prepared on the FTO substrate. In comparison, Fig. 1b shows a mp layer of anatase TiO_2 as a reference prepared on the same FTO substrate by sintering a commercial 18 NR-T paste at 500 °C. Here, average grain size of brookite and anatase TiO_2 are 18.5 ± 5.0 nm and 18.1 ± 5.3 nm, respectively. SEM images of brookite TiO_2 particles suspended in the precursor solution is given in Supplementary Fig. 1, which shows polyhedron shape of particles with substantially same size as in the above mp layer. We can see in Fig. 1a and 1b that sinter-free brookite TiO_2 forms more uniform and denser layer in comparison with sintered anatase TiO_2. Smooth surface of brookite mp layer is more clearly seen on atomic force microscopy (AFM) as exhibited in Fig. 1c and 1d. Here, the root mean square surface roughness (R_{ms}) of brookite layer was 9.09 nm while mp anatase layer gave rougher surface with R_{ms} of 14.59 nm. Strong connection of brookite particles are likely to cause flatter and more compact layer compared to anatase. Fig. 1e shows X-ray diffraction (XRD) patterns of the brookite mp layer. The brookite TiO_2 layer exhibits diffraction peaks at 2θ = 25.4°, 30.8°, 36.3°, 37.5°, 40.2°, 42.3°, 46.1°, 48.0° and 49.2°, which correspond to the diffraction pattern of brookite phase (ICDD 29-1360). The peak at 25.4° is the overlap of two peaks at 25.3° and 25.7° due to wide diffraction peak based on small crystal size of brookite layer. This result shows successful formation of brookite TiO_2 mp layers. The crystal size of brookite TiO_2 were 9.7 nm estimated by Sherrer equation[23] from the peak at 30.8°.

Photovoltaic films of perovskite, $MAPbI_{3-x}Cl_x$, were prepared based on the Cl-mixed single-step synthetic route and spin coating method as described previously.[4,6] Perovskite solar cells were fabricated by spin-coating spiro-OMeTAD as a hole-transport material (HTM) and by vacuum-depositing Au as a counter electrode. Cross-sectional images of the perovskite solar cells with brookite TiO_2 mp layers are shown in Fig. 2a. The average thickness of TiO_2 hole-blocking layer, mp TiO_2 layer and the perovskite layer were ~50 nm, ~250 nm

and ~300 nm, respectively. Photocurrent density-voltage (*J-V*) curves under irradiation of 100 mW cm^{-2} (AM 1.5) and incident photon to current conversion efficiency (IPCE) spectrum are shown in Fig. 2b and 2c, respectively. Photovoltaic characteristics obtained with four solar cells for each metal oxide structure are compared in Table 1.

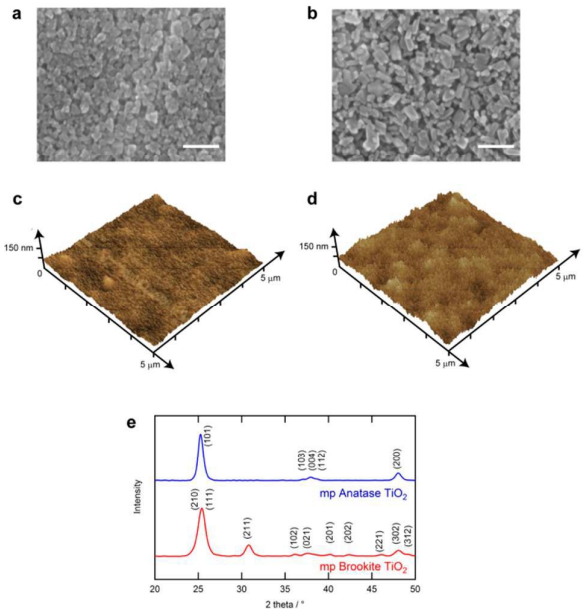

Figure 1. SEM observation for the morphologies of mp layers for (**a**) brookite TiO_2 particles (after 150 °C drying) and (**b**) anatase TiO_2 particles (after 500 °C sintering). 100-nm scale bars are shown in the figures. AFM surface images of (**c**) brookite TiO_2 mp layer and (**d**) anatase TiO_2 mp layer. (**e**) XRD diffraction patterns of brookite (red) and anatase (blue) TiO_2 mp layers. All samples were formed on FTO glass substrates.

Even though mp TiO_2 layer was prepared by sinter-less low temperature coating (130–150 °C), the brookite-based perovskite solar cells achieved the best performance with PCE up to 14.3%. High efficiency of the cell is supported by high V_{OC} and fill factor (*FF*). V_{OC} of the brookite-based cells, 0.97–1.00 V, is approximately 100 mV larger than that of conventional anatase mp TiO_2-based cells with equivalent structure and grain size. One reason for higher V_{OC} in brookite-based solar cells is the negative~~Here,~~ CB edge potential of brookite TiO_2 ~~is assumed to be more negative than~~ compared to anatase (0.01–0.19 eV more negative,[17] Supplementary Fig. 3)~~ and lead to enhance V_{OC}~~. Electron selective semiconductors of more negative CB edge can result in decrease in short-circuit photocurrent density (J_{SC}) due to less driving energy of electron injection from perovskite layer.[11,24] However, the brookite TiO_2-based solar cells exhibit J_{SC} equivalent to those of the anatase TiO_2 cells by maintaining high value (~20 mA cm^{-2}). This relation is demonstrated by IPCE showing equal characteristics (70–80%). Taking into account the distribution of density-of-state in CB, higher CB level of brookite can still accept electrons from CB edge of $MAPbI_{3-x}Cl_x$ (~3.9 eV vs. vacuum[1]) when carrier transfer across the TiO_2-perovskite interface is enhanced by good structural continuity of hetero-junction which we expect for the brookite TiO_2. N.-G. Park et al. has compared rutile and anatase TiO_2 mp layer as an electron collection layer for perovskite solar cells.[25] Rutile TiO_2, which has low electron conductivity, exhibits slower recombination than anatase but V_{OC} was lower than anatase due to more positive CB edge potential. In this study, brookite, which has low electron conductivity[19] and negative CB edge potential, may decrease recombination without causing voltage loss and result in high V_{OC} and *FF*.

It is known that perovskite solar cells exhibit high PCE even with use of insulating mp layer such as Al_2O_3.[4,6,26] In this case, the insulating mp layer, incapable of electron collection, works only as a scaffold for perovskite crystal growth. Here large carrier diffusion lengths of $MAPbI_{3-x}Cl_x$ (>μm[27-29]) enables excited electrons to diffuse through perovskite layer (~300 nm) and directly transfer to a TiO_2 hole-blocking layer on FTO electrode.[4] The absence of carrier transfer across the interface of mp layer and perovskite is assumed to give small voltage loss and relatively high V_{OC}. For comparison, we have also examined a perovskite cell made on a mp Al_2O_3 as the scaffolds, in which the mp layer of Al_2O_3 was prepared by high temperature sintering (500 °C) similar to anatase TiO_2. For this reference cell, thickness (~250 nm) and grain size (19.7 ± 4.6 nm, estimated by SEM observation (Supplementary Fig. 2)) was adjusted as similar to brookite mp layer. The result showed that the Al_2O_3-based cell can generate high V_{OC} compared to brookite-based cell. However, the cell exhibited low *FF* and was accompanied by significant hysteresis in *J-V* characteristics (Fig. 2b and Table 1). Low *FF* may reflect increase in internal resistance due to non-conductive Al_2O_3 scaffold and long distance carrier diffusion through perovskite layer. The series resistance estimated from *J-V* curves at V_{OC} was 53 ± 8 Ω and 73 ± 7 Ω (n = 4) for perovskite solar cells with brookite TiO_2 and Al_2O_3, respectively. As a result, brookite TiO_2 yielded higher efficiency backed by high *FF*, which reflects efficient electron injection from perovskite to the brookite TiO_2. It is noteworthy that low-temperature processed brookite TiO_2 electron collector can maintain high *FF* and low internal resistance to achieve efficiency more than those obtained by sintered mp TiO_2 and Al_2O_3.

Table 1. Photovoltaic performance of perovskite cells with brookite TiO_2 (non-sintered), anatase TiO_2 (sintered) and Al_2O_3 (sintered) mp layers. Data collected for each 4 cells

Scan direction	Mesoporous layer	J_{SC} [mA cm^{-2}]	V_{OC} [V]	Fill factor	PCE [%]
Forward −0.1 V ↓ 1.1 V	Brookite TiO_2	20.2 ± 0.6	0.98 ± 0.01	0.69 ± 0.01	13.5 ± 0.6
	Anatase TiO_2	19.4 ± 1.4	0.87 ± 0.01	0.62 ± 0.01	10.3 ± 0.7
	Al_2O_3	19.2 ± 1.3	1.05 ± 0.02	0.55 ± 0.03	11.0 ± 0.8
Backward 1.1 V ↓ −0.1 V	Brookite TiO_2	20.0 ± 0.6	0.99 ± 0.01	0.67 ± 0.03	13.3 ± 1.0
	Anatase TiO_2	19.4 ± 1.4	0.90 ± 0.01	0.66 ± 0.01	11.5 ± 0.6
	Al_2O_3	18.5 ± 1.6	1.05 ± 0.02	0.66 ± 0.05	12.7 ± 0.3

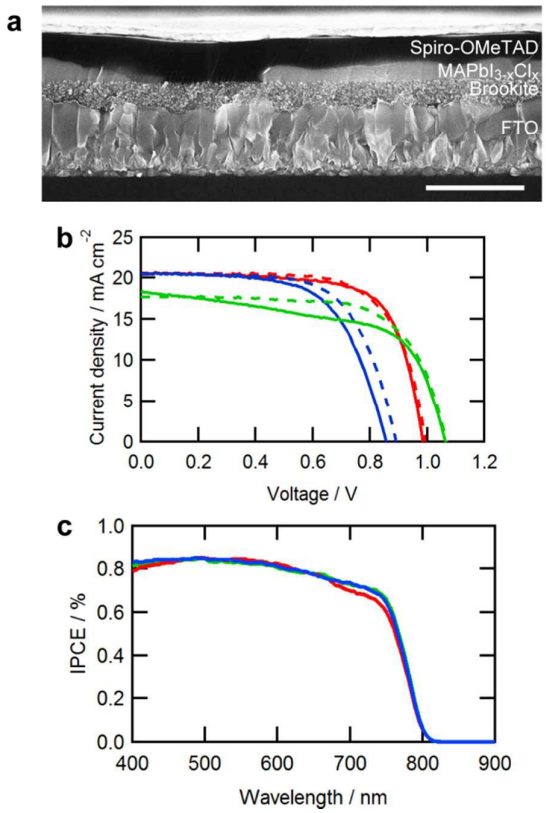

Figure 2. (**a**) A cross-sectional SEM image of perovskite solar cells with brookite TiO_2 mp layer. A 1-μm scale bar is shown. (**b**) Photocurrent density-voltage (*J-V*) curves and (**c**) incident photon to current conversion efficiency (IPCE) spectra for perovskite solar cells with anatase TiO_2 (sintered at 500 °C, blue), brookite TiO_2 (dried at 150 °C, red) and Al_2O_3 (sintered at 500 °C, green) mp layers. Forward (–0.1 V → 1.1 V) and backward (1.1 V → –0.1 V) scans are indicated as solid and deted lines, respectively.

On the other hand, the morphology and crystalline quality of perovskite layer being affected by the underlying mp TiO_2 layer strongly affect the solar cell performance.[30,31] In addition to high V_{OC}, other significant nature of brookite TiO_2 as mp collector is hysteresis-less performance in perovskite cells. The anatase-based cell exhibits hysteretic *J-V* curves that give larger current density for backward scan (from –0.1 V to 1.1 V direction) than forward scan (from 1.1 V to –0.1 V) (Fig. 2b). In contrast, brookite-based cell always exhibited *J-V* curves with little or no hysteresis. *FF* was also improved in the hysteresis-less *J-V* curves. This difference can be explained by morphology of perovskite layer formed on mp layers. The surface morphologies of perovskite layers on the anatase and brookite mp layers were displayed in Fig. 3a and 3b. While the interiors of the both mp TiO_2 layers were filled with perovskite, excess of perovskite is covering the surface of mp layers. Here, the surface of anatase TiO_2 mp layer was partially covered (capped) with perovskite layer. In contrast, the surface of brookite TiO_2 layer was fully covered with large grain perovskite layer, showing dramatic improvement in surface coverage. In the mesoscopic structure, the high coverage of perovskite on mp layer reduces contact and electrical leakage between mp layer and HTM and enhances V_{OC} and *FF*. XRD profiles of perovskite layers formed on the mp layers were shown in Fig. 3c. Characteristic peaks of $MAPbI_{3-x}Cl_x$ perovskite layer at 14.2° and 28.5° based on diffraction at (110) and (220) planes[32] were observed for perovskite formed on the both mp layers. We estimated perovskite crystal size from the diffraction peak at 14.2° with Scherrer equation.[23] The crystal diameter of perovskite was 81.5 nm on brookite mp layer, which was more than twice the size, 33.8 nm, obtained for anatase mp layer. Further, narrower diffraction bands and higher intensity indicate that the perovskite layer formed on brookite TiO_2 has higher crystallinity than that on anatase TiO_2. For the hysteresis-less performance of brookite TiO_2 cells, we consider that large grain size of perovskite with less grain boundary of perovskite is improving the interfacial structure at heterojunction between TiO_2 and perovskite that we found to play a role of causing hysteresis.[33,34] Such difference in perovskite crystal morphology may be ascribed to the different property in crystal phase of TiO_2. For example, water contact angle of mp anatase and brookite were measured to be 7.7 ± 0.8° and 1.4 ± 0.1°, respectively (n = 3), for the films of Fig. 1c and 1d. Higher hydrophilicity of the brookite surface showed apparently quicker spread of water on the surface. Since hydrophilic surface increases the adhesion of perovskite crystal on semiconductor layer,[35] the large crystal size and high surface coverage of perovskite was achieved on brookite TiO_2. The active brookite surface,[36-39] such as (210) plane, may be the cause of adhesive characteristics of mp brookite surface.

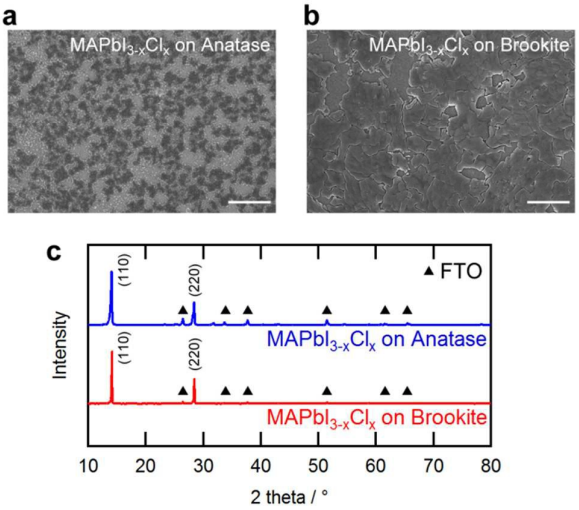

Figure 3. Surface SEM images of $MAPbI_{3-x}Cl_x$ layers formed on (**a**) anatase and (**b**) brookite TiO_2 mp layers. A 10-μm scale bars are shown in the figures. (**c**) XRD patterns of $MAPbI_{3-x}Cl_x$ layers formed on anatase and brookite TiO_2 mp layers. ▲ in Figure 3c indicates diffraction peaks due to FTO.

Conclusions

In conclusion, we have employed brookite TiO_2 for a conductive mp scaffold for perovskite solar cells. Significant advantage of brookite TiO_2 is addressed to low-temperature solution processability without losing but even improving the efficiency of perovskite solar cell. Low temperature fabrication

of $MAPbI_{3-x}Cl_x$ solar cell with brookite TiO_2 mp collector achieved PCE up to 14.3% without hysteretic behavior in photovoltaic performance. In comparison with conventional anatase mp TiO_2, V_{OC} was improved by ~100 mV in the brookite-based perovskite cell. The brookite layer works as an excellent scaffold for uniform crystallization of perovskite by achieving high surface coverage with large crystal grains, which can increase *FF* and reduce hysteresis in *J-V* curves of solar cells. We could also fabricate brookite-based flexible perovskite solar cells on plastic substrates, which will be reported elsewhere.

Acknowledgements

This study was supported by Japan Science and Technology Agency (JST) Advanced Low Carbon Technology R&D program (ALCA). T. M. thanks the support of Japanese Society for Promotion of Science (JSPS) Grant-in-Aid for Scientific Research B Grant Number 26289265. We appreciate Prof. Tetsu Tatsuma and Mr. Yoshinori Kuroiwa for contact angle measurement. We appreciate Prof. Hiroshi Segawa for allowing access to research facilities at Research Center for Advanced Science and Technology (RCAST), the University of Tokyo. We appreciate Dr. Hideo Kogure for valuable discussions.

References

1 A. Kojima, K. Teshima, Y. Shirai and T. Miyasaka, *J. Am. Chem. Soc.*, 2009, **131**, 6050-6051.
2 H. Zhou, Q. Chen, G. Li, S. Luo, T. Song, H.-S. Duan, Z. Hong, J. You, Y. Liu and Y. Yang, *Science*, 2014, **345**, 542-546.
3 N. J. Jeon, J. H. Noh, W. S. Yang, Y. C. Kim, S. Ryu, J. Seo and S. I. Seok, *Nature*, 2015, **517**, 476-480.
4 M. M. Lee, J. Teuscher, T. Miyasaka, T. N. Murakami and H. J. Snaith, *Science*, 2012, **338**, 643-647.
5 J. Burschka, N. Pellet, S.-J. Moon, R. Humphry-Baker, P. Gao, M. K. Nazeeruddin and M. Grätzel, *Nature*, 2013, **499**, 316-319.
6 T. Miyasaka, *Chem. Lett.*, 2015, **44**, 720-729.
7 H.-S. Kim, J.-W. Lee, N. Yantara, P. P. Boix, S. A. Kulkarni, S. Mhaisalkar, M. Grätzel and N.-G. Park, *Nano Lett.*, 2013, **13**, 2412-2417.
8 M. H. Kumar, N. Yantara, S. Dharani, M. Graetzel, S. Mhaisalkar, P. P. Boix and N. Mathews, *Chem. Commun.*, 2013, **49**, 11089-11091.
9 J. Song, E. Zheng, J. Bian, X.-F. Wang, W. Tian, Y. Sanehira and T. Miyasaka, *J. Mater. Chem. A*, 2015, **3**, 10837-10844.
10 K. Mahmood, B. S. Swain, A. R. Kirmani and A. Amassian, *J. Mater. Chem. A*, 2015, **3**, 9051-9057.
11 A. Bera, K. Wu, A. Sheikh, E. Alarousu, O. F. Mohammed and T. Wu, *J. Phys. Chem. C*, 2014, **118**, 28494-28501.
12 Y. Ogomi, A. Morita, S. Tsukamoto, T. Saitho, Q. Shen, T. Toyoda, K. Yoshino, S. S. Pandey, T. Ma and S. Hayase, *J. Phys. Chem. C*, 2014, **118**, 16651–16659.
13 Y. C. Shih, L. Y. Wang, H. C. Hsieh and K. F. Lin, *J. Mater. Chem. A*, 2015, **3**, 9133-9136.
14 L. Zuo, Z. Gu, T. Ye, W. Fu, G. Wu, H. Li and H. Chen, *J. Am. Chem. Soc.*, 2015, **137**, 2674-2679.
15 P. Docampo, J. M. Ball, M. Darwich, G. E. Eperon and H. J. Snaith, *Nat. Commun.*, 2013, **4**, 2761.
16 T. Miyasaka, M. Ikegami and Y. Kijitori, *J. Electrochem. Soc.*, 2007, **154**, A455-A461.
17 A. D. Paola, M. Bellardita and L. Palmisano, *Catalysts*, 2013, **3**, 36-73.
18 C. Magne, S. Cassaignon, G. Lancel and T. Pauporté, *ChemPhysChem*, 2011, **12**, 2461-2467.
19 Y. Kusumawati, M. Hosni, M. A. Martoprawiro, S. Cassaignon and T. Pauporté, *J. Phys. Chem. C*, 2014, **118**, 23459-23467.
20 J. Xu, K. Li, S. Wu, W. Shi and T. Peng, *J. Mater. Chem. A*, 2015, **3**, 7453-7462.
21 K. Miyoshi, M. Numao, M. Ikegami and T. Miyasaka, *Electrochemistry*, 2008, **76**, 158-160.
22 S. Morita, M. Ikegami, T.-C. Wei and T. Miyasaka, *ChemPhysChem*, 2014, **15**, 1190-1193.
23 A. L. Patterson, *Phys. Rev.*, 1939, **56**, 978-982.
24 A. Kogo, Y. Numata, M. Ikegami and T. Miyasaka, *Chem. Lett.*, 2015, **44**, 829-830.
25 J.-W. Lee, T.-Y. Lee, P. J. Yoo, M. Grätzel, S. Mhaisalkar and N.-G. Park, *J. Mater. Chem. A*, 2014, **2**, 9251-9259.
26 J. M. Ball, M. M. Lee, A. Hey and H. J. Snaith, *Energy Environ. Sci.*, 2013, **6**, 1739-1743.
27 S. D. Stranks, G. E. Eperon, G. Grancini, C. Menelaou, M. J. P. Alcocer, T. Leijtens, L. M. Herz, A. Petrozza, H. J. Snaith, *Science*, 2013, **342**, 341-344.
28 E. Edri, S. Kirmayer, S. Mukhopadhyay, K. Gartsman, G. Hodes and D. Cahen, *Nat. Commun.*, 2014, **5**, 3461.
29 D. Shi, V. Adinolfi, R. Comin, M. Yuan, E. Alarousu, A. Buin, Y. Chen, S. Hoogland, A. Rothenberger, K. Katsiev, Y. Losovyj, X. Zhang, P. A. Dowben, O. F. Mohammed, E. H. Sargent, O. M. Bakr, *Science*, 2015, **347**, 519-522.
30 G. E. Eperon, V. M. Burlakov, P. Docampo, A. Goriely and H. J. Snaith, *Adv. Funct. Mater.*, 2014, **24**, 151–157.
31 T.-B. Song, Q. Chen, H. Zhou, C. Jiang, H.-H. Wang, Y. Yang, Y. Liu, J. You and Y. Yang, *J. Mater. Chem. A*, 2015, **3**, 9032–9050.
32 A. Dualeh, N. Tétreault, T. Moehl, P. Gao, M. K. Nazeeruddin and M. Grätzel, *Adv. Funct. Mater.*, 2014, **24**, 3250-3258.
33 Y. Shao, Z. Xiao, C. Bi, Y. Yuan and J. Huang, *Nat. Commun.*, 2014, **5**, 5784.
34 A. K. Jena, H.-W. Chen, A. Kogo, Y. Sanehira, M. Ikegami and T. Miyasaka, *ACS Appl. Mater. Interfaces*, 2015, **7**, 9817-9823.
35 L. Cojocaru, S. Uchida, Y. Sanehira, J. Nakazaki, T. Kubo and H. Segawa, *Chem. Lett.*, 2015, **44**, 674-676.
36 W.-K. Li, X.-Q. Gong, G. Lu and A. Selloni, *J. Phys. Chem. C*, 2008, **112**, 6594-6596.
37 M. M. Rodriguez, X. Peng, L. Liu, Y. Li and J. M. Andino, *J. Phys. Chem. C*, 2012, **116**, 19755-19764.
38 W. Yan, B. Chen, S. M. Mahurin, S. Dai and S. H. Overbury, *Chem. Commun.*, 2004, 1918-1919.
39 W. Yan, B. Chen, S. M. Mahurin, V. Schwartz, D. R. Mullins, A. R. Lupini, S. J. Pennycook, S. Dai and S. H. Overbury, *J. Phys. Chem. B*, 2005, **109**, 10676-10685.

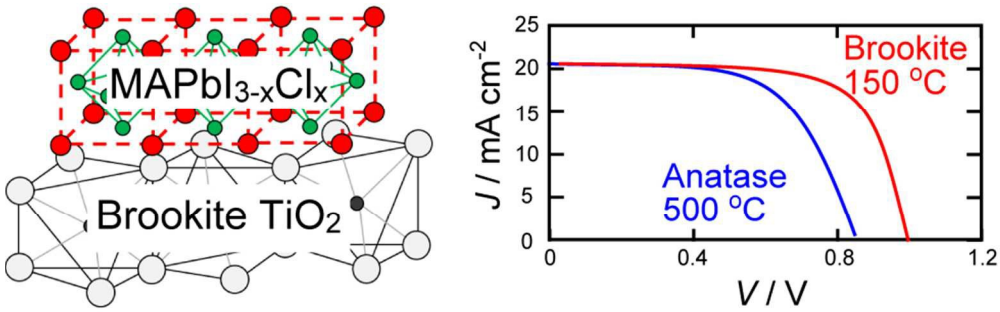

82x26mm (300 x 300 DPI)